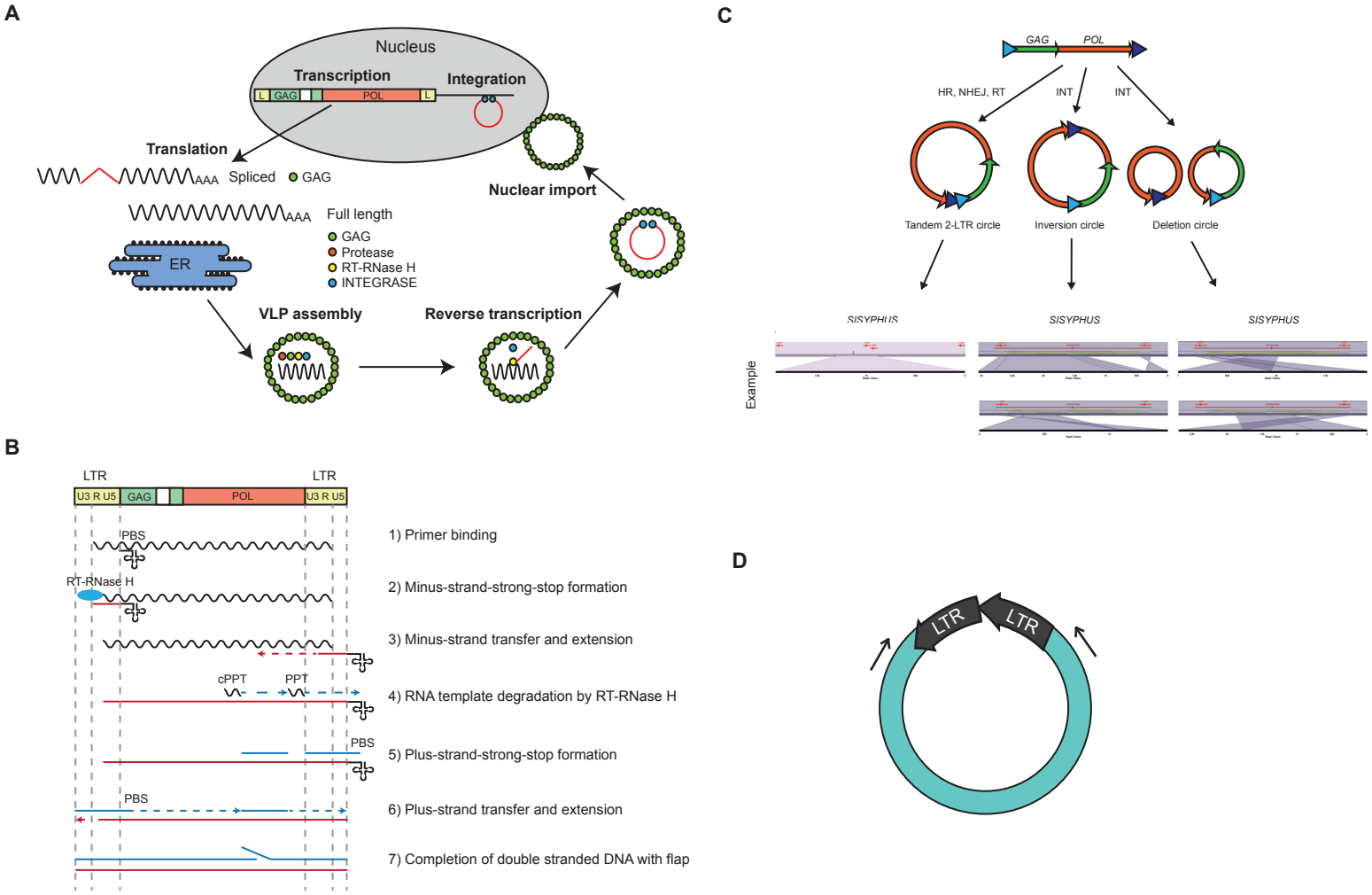

Supplemental Figure S1. Replication cycle of LTR retrotransposon in plants. (A) Production of virus-like-particles (VLPs) is initiated by transcription of functional elements. For *COPIA* elements in Arabidopsis, introns are spliced from subgenomic RNA to make only GAG proteins (Oberlin et al., 2017). Polyproteins encoded by full-length RNA comprise enzymes essential for reverse transcription and integration. After polyproteins are cleaved by protease, RT-RNase H processes full-length genomic RNA by reverse transcription. Double-stranded VLP DNA enters the nucleus and inserts into new genomic loci mediated by integrase. Abbreviations: L, LTR; ER, endoplasmic reticulum (B) Reverse transcription is initiated by tRNA primers that bind to the primer binding site (PBS). Minus-strand strong-stop DNA is made, transferred to the 3' LTR, and extended toward to 5' end. After removal of genomic RNA by RT-RNase H, RNA polypurine tract (PPT) fragments resistant to digestion are used for plus-strand strong-stop DNA formation. Plus-strand strong-stop DNA is transferred to 5' LTR and extended. Central PPTs (cPPT) produce additional plus-strand DNA that forms a flap structure by invasion of the extended plus-strand DNA from 5' end. (C) Examples of circular VLP DNA formation. Diagrams of circular VLP DNA formation (modified from Garfinkel et al., 2006) are shown to illustrate different types of products by homologous recombination (HR), nonhomologous end joining (NHEJ), reverse transcription (RT), or integrase (IN). Examples of Oxford Nanopore read alignments to *SISYPHUS* are shown for each circular DNA type using Ribbon (http://biorxiv.org/content/early/2016/10/20/082123). (D) Inverse PCR for circular DNA detection. Arrows indicate the orientations of two primers.

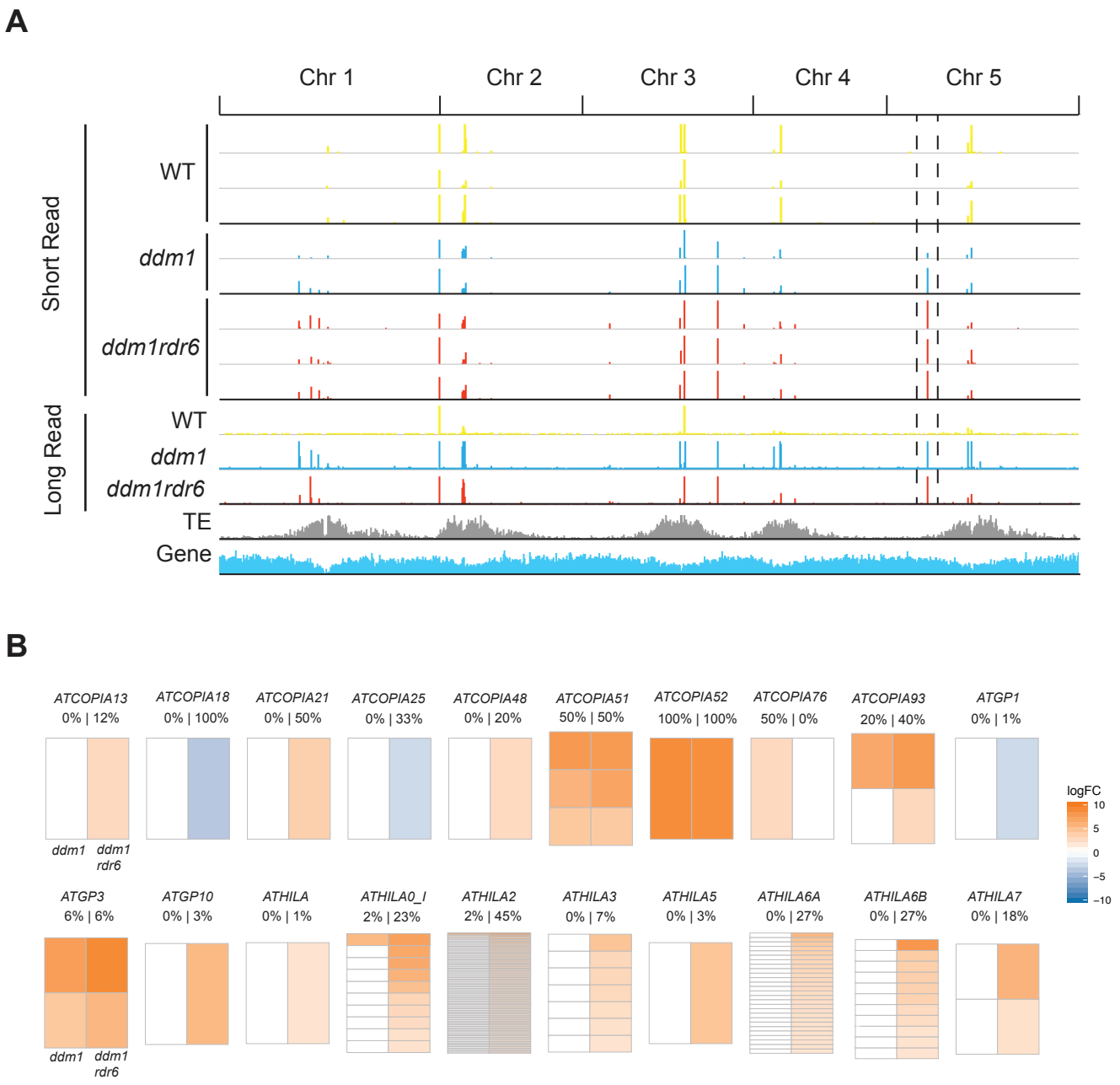

Supplemental Figure S2. Genome-wide analyses of VLP DNA products in *ddm1* and *ddm1rdr6*. (A) 3 replicate libraries of short sequencing reads (Illumina) and long sequencing reads (Oxford Nanopore) from VLP DNA samples were aligned to the Arabidopsis genome. Peaks of read alignments unique to *ddm1* and *ddm1rdr6* correspond to LTR retrotransposon loci that produce VLP DNA, whereas wild-type (WT) samples share DNase-insensitive background regions. Dashed lines indicate *EVADE*. Density of transposable elements (TE) and genes is shown. (B) Heat maps of log2 fold changes of VLP DNA enrichment in *ddm1* and *ddm1rdr6* for LTR retrotransposons. Each *ddm1* and *ddm1rdr6* genotype was compared to WT to calculate fold changes from short-read replicate samples. The percentages of significantly enriched TEs within the family for each genotype are shown above the heatmaps.

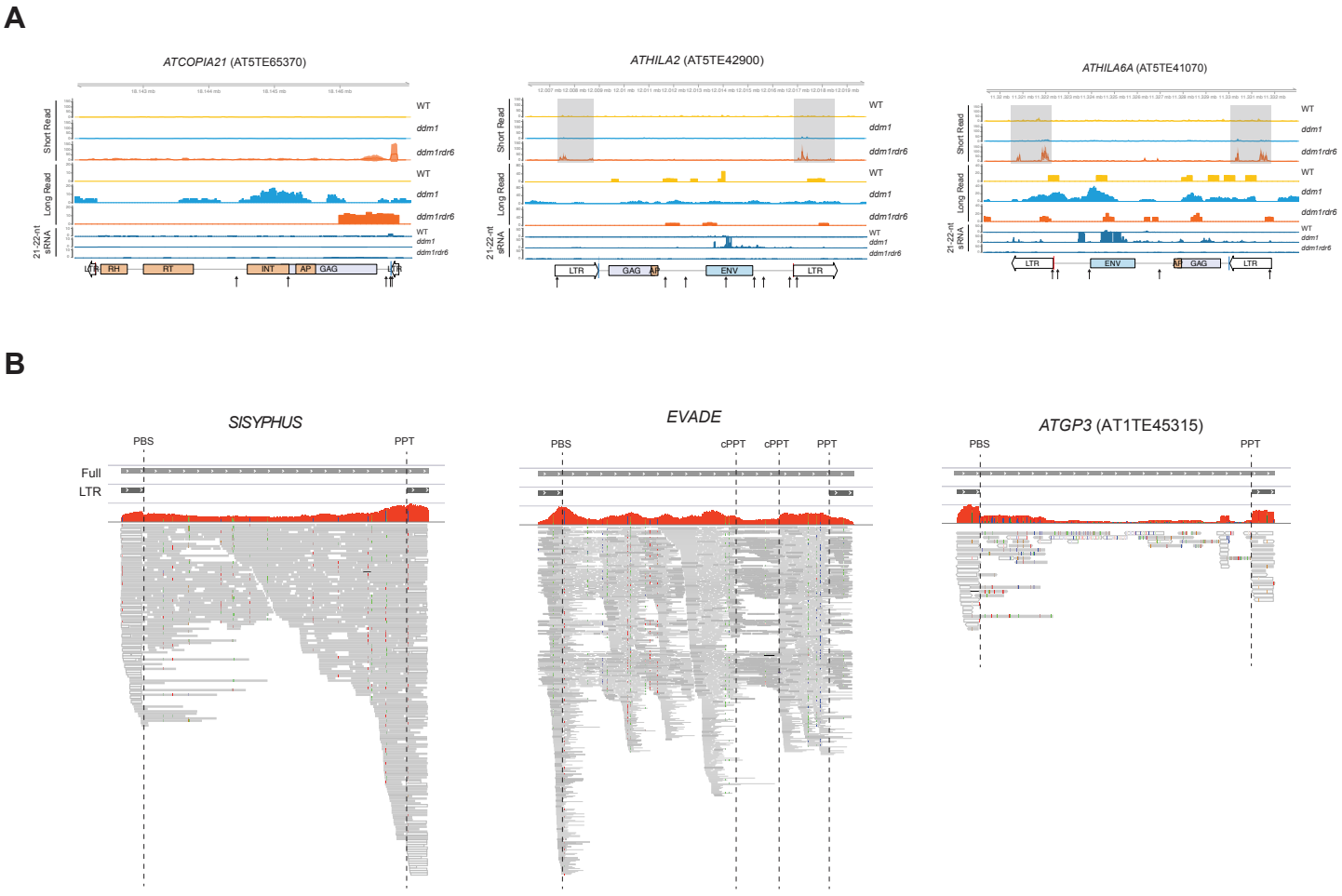

Supplemental Figure S3. Additional VLP DNAseq data. (A) Representative LTR retrotransposons significantly enriched in VLP DNA of *ddm1rdr6* plants. Short read (Illumina) VLP sequences were aligned to transposons, and mean read counts per million mapped and 95% confidence intervals of biological replicates are shown for wild-type (WT; yellow), *ddm1* (blue), and *ddm1rdr6* (orange) (n=3 for WT and *ddm1rdr6*; n=2 for *ddm1*). Gray shadow indicate the region showing partial VLP DNA from *ATHILA* elements. Long read sequence coverage was determined in a similar way from pooled VLP DNA replicates for each genotype and sequenced as one replicate by the long read sequencing platform. Annotation, small RNA, PBS and PPT sites are as in Figs. 1B, 6B. Target positions of miRNAs are indicated as arrows (see Supplemental Table S4 for details). (B) Alignments of long sequencing reads from VLP DNA in *ddm1rdr6*. Alignments are shown for *SISYPHUS* (AT3TE76225), *EVADE* (AT5TE20395), and *ATGP3* (AT1TE45315) VLP DNA. PBS, PPT, and cPPT positions are indicated as dashed lines relative to full and LTR annotation. Sequencing gaps and mismatches are indicated as in Fig. 3.

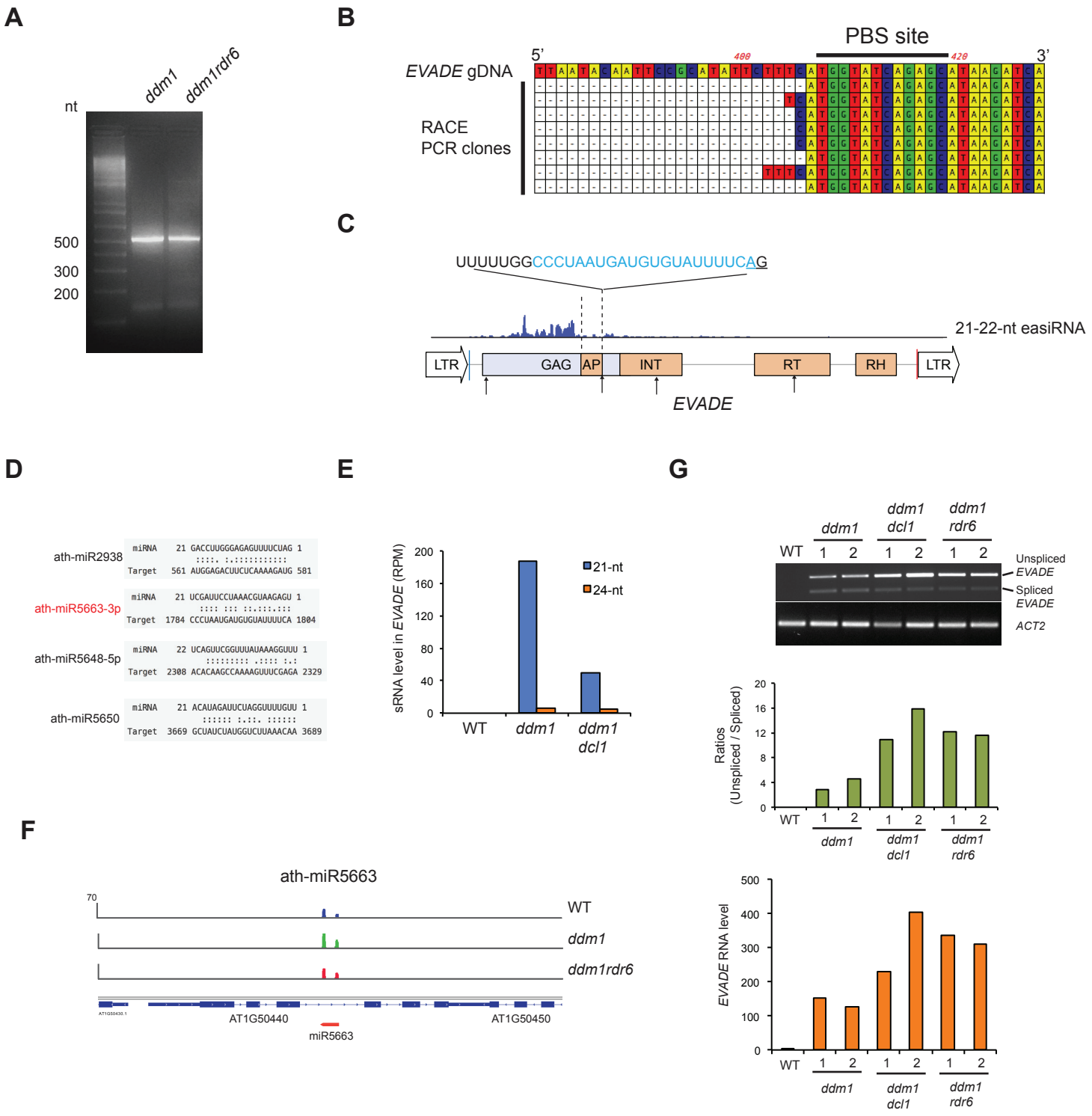

Supplemental Figure S4. MicroRNAs targeting GAG and integrase (IN) regions of *EVADE*. (A) 5' RACE PCR products from *ddm1* and *ddm1rdr6* using primers in the *EVADE* GAG gene. (B) 5' end sequences from the RACE products of *ddm1* (n=8) indicate RNaseH cleavage immediately upstream of the PBS. (C) miRNA target sites predicted by psRNATarget (Dai et al., 2018) are shown as arrows. 21-22-nt easiRNAs and *EVADE* annotation are as in Fig. 1. Dashed lines indicate the intron of *EVADE*. The underlined and blue letters indicate the splicing acceptor AG nucleotide sequence and the target sequence of ath-miR5663-3p, respectively. (D) Sequence alignments of miRNAs with *EVADE* as a target sequence. (E) *EVADE* easiRNA abundance in reads per million (RPM) in wild-type (WT), *ddm1*, and *ddm1dcl1* mutants using a public dataset (GSE52951) (Creasey et al., 2014). (F) ath-miR5663 is detected in inflorescence tissues of wild-type (WT), *ddm1*, and *ddm1rdr6* (Creasey et al., 2014). (G) RT-PCR of *EVADE* for detection of spliced and unspliced forms in *ddm1*, *ddm1dcl1*, and *ddm1rdr6* (Top panel). Ratios of unspliced/spliced were calculated using band intensity from RT-PCR. *EVADE* RNA levels normalized by *ACT2* were obtained using RT-qPCR for each genotype (Bottom panel).

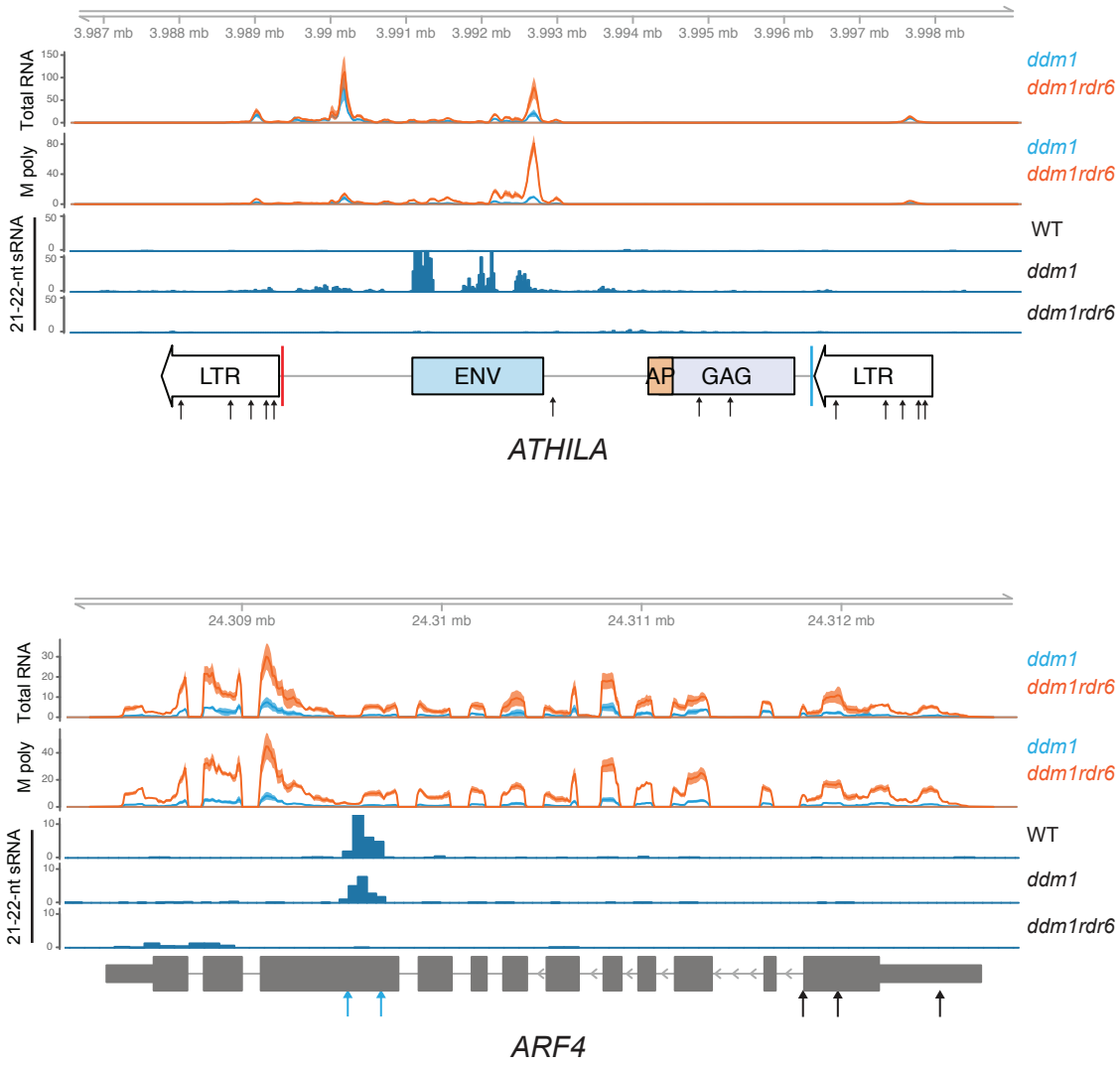

Supplemental Figure S5. Polysomal occupancy of mRNA in *ddm1* and *ddm1rdr6*. Total RNA and microsome-polysomal RNA (M poly) tracks are shown for *ATHILA* (AT4TE17360) and *ARF4* (AT5G60450), with annotation and 21-22-nt easiRNA are as in Fig. 1. Black arrows indicate predicted miRNA target sites (Supplemental Table S4). Two target sites of the transacting small interfering RNA, tasiR-ARF4 are indicated as blue arrows (Williams et al., 2005).

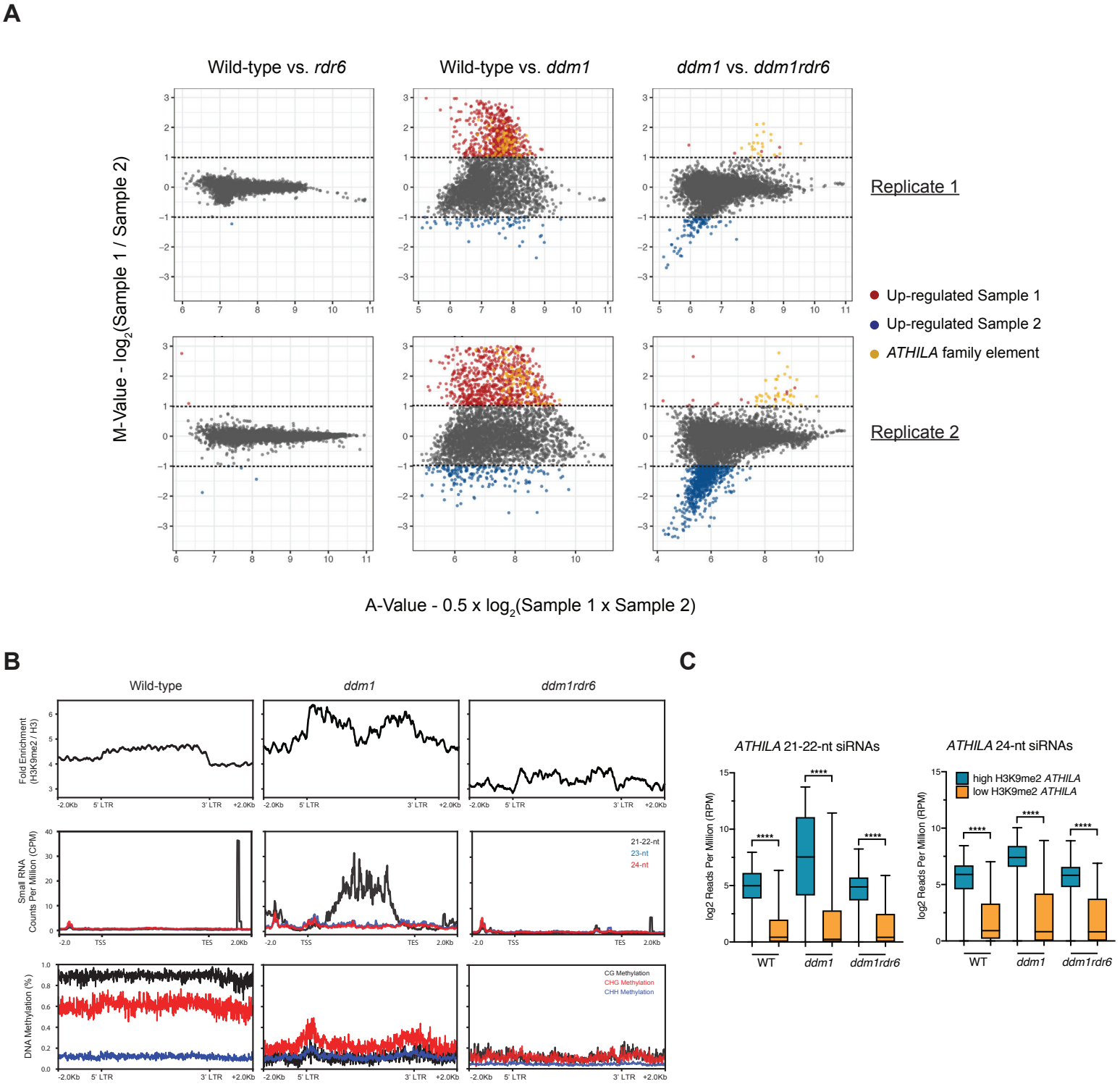

Supplemental Figure S6. Meta-analysis of H3K9me2, small RNAs, and DNA methylation. (A) MA plots of H3K9me2 ChIPseq data for wild-type, *ddm1*, and *ddm1rdr6*. Pairwise comparisons between genotypes revealing global changes in H3K9me2. log2 fold changes between Sample 1 and Sample 2 (M-value) are plotted against average read density between samples (A-value). Points represent ChIP-seq peaks that are up-regulated in Sample 1 (red), up-regulated in Sample 2 (blue), or not significantly different (gray). Annotated *ATHILA* family elements that are differentially regulated between samples are highlighted in yellow. (B) Metaplots depicting H3K9me2, small RNAs, and DNA methylation levels at the 73 most significantly affected *ATHILA* family elements across wild type, *ddm1*, and *ddm1rdr6* genotypes. Small RNA and DNA methylation data were obtained from a previously published study (Creasey et al., 2014). (C) Direct comparison of small RNA abundances between *ATHILA* family elements that gain RDR6-dependent H3K9me2 in *ddm1* and those that do not. Both 21-22-nt and 24-nt small RNA levels are shown in log2 reads per million (RPM) across wild-type (WT), *ddm1*, and *ddm1rdr6* genotypes. A two-sample Kolmogorov–Smirnov test was used to compare differences between *ATHILA* classes (**** p-value < 0.0001).

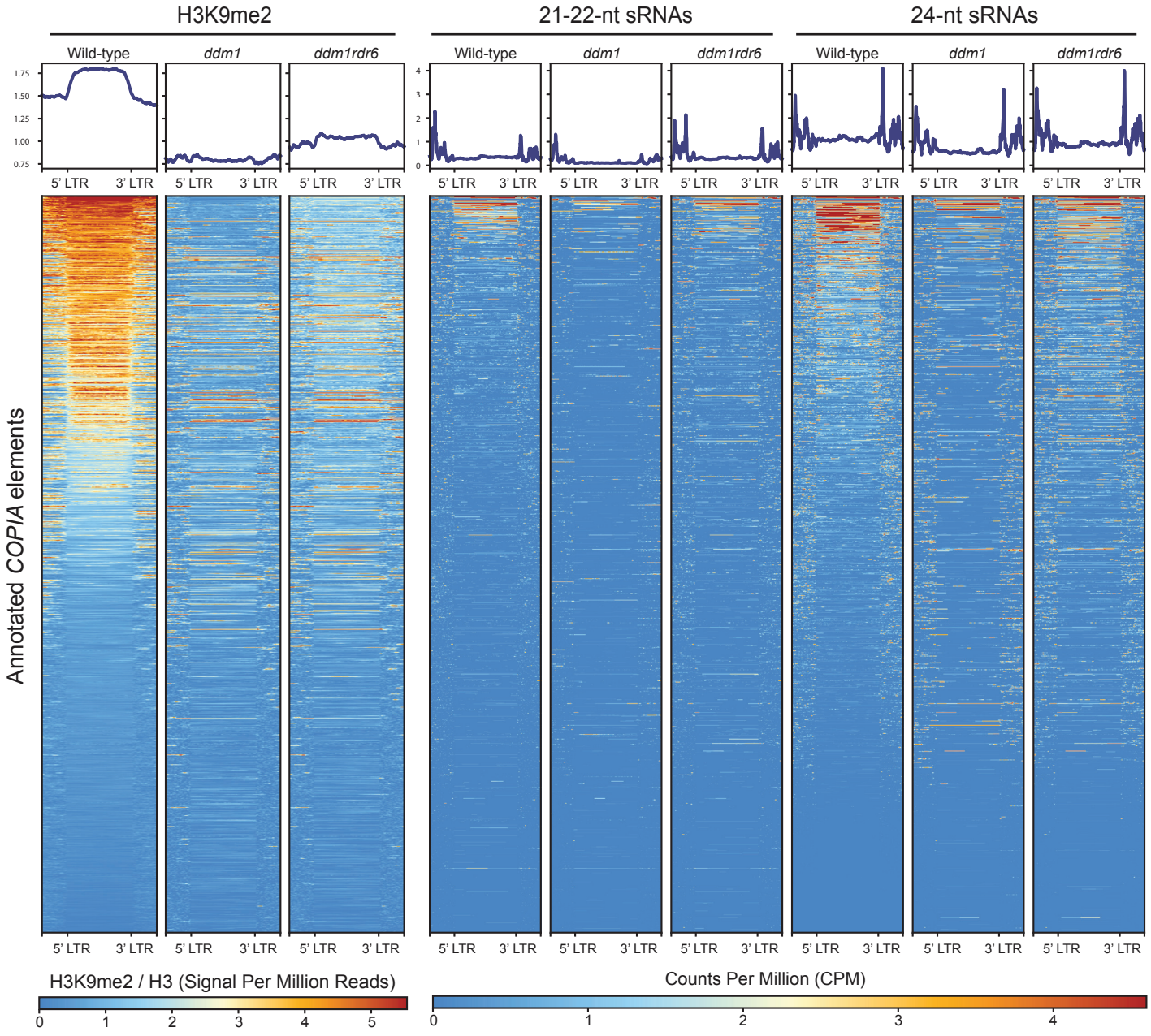

Supplemental Figure S7. Up-regulation of H3K9me2 at *COPIA* family loci in *ddm1rdr6* as compared to *ddm1*. H3K9me2 signal at transposable elements from multiple *COPIA* families was analyzed across wild-type (WT), *ddm1*, and *ddm1rdr6* genotypes and correlated with previously published small RNA data (Creasey et al., 2014).